

A continuous flow generator of organic hypochlorites for the neutralization of chemical warfare agent simulants†

Victor-Emmanuel H. Kassin, ^{‡,a} Diana V. Silva Brenes, ^{‡,a,b} Thomas Bernard,^a Julien Legros ^c and Jean-Christophe M. Monbaliu ^{*,a}

Herein, we report the development of a continuous flow generator that produces highly reactive organic hypochlorites for the chemical neutralization of sulfur-based chemical warfare agent (CWA) simulants. The generator relies on resource and equipment with low environmental footprint and uses chemicals that are widely available and cheap. The standard decontamination protocol for sulfur-based CWA "mustard gas" (a.k.a. Yperite or **HD**) relies on bleach (aqueous sodium hypochlorite) as a convenient oxidative neutralization measure; however, the high lipophilicity of **HD** causes the formation of micelles and hence superficial and/or unselective detoxification. Aqueous bleach can be rapidly upgraded to more lipophilic organic hypochlorites (**MeOCl**, **EtOCl**, **iPrOCl** and **tBuOCl**). We demonstrate that the latter readily oxidize simulants of **HD** (such as chloroethyl ethyl sulfide (**CEES**)) to the corresponding sulfoxide (**CEESO**). With a fine tuning of the reaction conditions, the oxidation is nearly instantaneous and prevents the formation of toxic overoxidized sulfones, though organic hypochlorites also contribute to the innocuous chlorination of the neutralized sulfoxide. The assets of continuous flow technology enable the merging of both the upstream hypochlorite generator and the downstream neutralization setup to provide a safe, compact and mobile framework. Some aspects of the reactivity of organic hypochlorites with model sulfur compounds are also discussed by means of computational chemistry (DFT). The flexibility (simple chemicals, liquid feeds and wastes) and efficiency (space time yield = $3.74 \text{ kg L}^{-1} \text{ h}^{-1}$) of this protocol outclass other recently reported neutralization procedures in flow.

Received 3rd February 2022,
Accepted 11th March 2022
DOI: [10.1039/d2gc00458e](https://doi.org/10.1039/d2gc00458e)
rsc.li/qreenchem

Introduction

The development of new neutralization protocols on chemical warfare agent (CWA) simulants (as well as on actual CWAs with military clearance) has attracted increasing attention from the Chemical and Chemical Engineering communities, as evidenced by an increasing number of reviews and original articles over the past 10 years.¹⁻¹⁸ This is somehow paradoxical, yet easily justifiable with the current background threat of

terror attacks, as well as alleged reports of the use of CWA targeting both entire populations or individuals. The Chemical Weapons Convention (CWC) bans since 1993 the possession, manufacture, and use of CWAs and all their precursors.^{19,20} However, despite being ratified in 1997 by over 193 countries, large inventories of CWAs are still stockpiled across the world. All this justifies the investment of resources and the development of research programs aiming at the detection and/or the chemical neutralization of CWAs.^{14-18,21-28} Mustard gas (**HD**, 1-chloro-2-[(2-chloroethyl)sulfanyl] ethane, CAS 505-60-2, Fig. 1) is a viscous liquid with vesicant (blistering) properties that causes severe damage to the eyes, skin, and respiratory tract. **HD** also damages cells as a strong alkylating agent and can affect the nervous system upon acute exposure.

The most common destruction of HD is through incineration at dedicated facilities,²⁹ which comes with significant safety concerns associated with its transportation. An emerging and inherently safer strategy relies on a chemical decontamination to form less toxic compounds prior to incineration. Three main chemical neutralization protocols are reported in the literature: oxidation, hydrolysis and dehydrohalogenation.

^aCenter for Integrated Technology and Organic Synthesis, MolSys Research Unit, University of Liège, B-4000 Liège (Sart Tilman), Belgium.
E-mail: ic.morabito@uliege.be; <https://www.citos.uliege.be>

*E-mail: jc.monballu@uliege.be; <https://www.citos.uliege.be>
^bCrystallization Design Institute, Molecular Sciences Research Center, University of Puerto Rico, 1290 Ponce De León Ave, San Juan, PR 00926, USA*

^cNormandie Université, INSA Rouen, UNIROUEN,
CNRS COBRA Laboratory (UMR 6014 & FR3038), 76000 Rouen, France

† Electronic supplementary information (ESI) available: Fluidic

† Electronic supplementary information (ESI) available: Fluidic component experimental procedures, details of the fluidic setup and procedures, operational details, details for the off-line analyses (GC, HPLC) and structure assignments (NMR). See <https://doi.org/10.1039/d2ra00458a>.

assignments (NMR). S
† Equal contributions

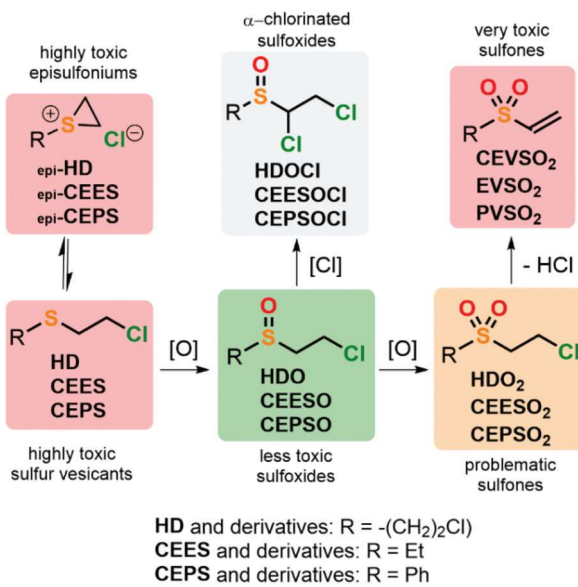


Fig. 1 Reactivity of HD and common simulants under oxidative neutralization conditions.

These neutralization protocols aim at disrupting the formation of a electrophilic episulfonium species (Fig. 1), the formation of which is associated with the acute toxicity of sulfur mustards. Among the neutralization methods, the oxidative neutralization of **HD** (or its relevant simulants 2-chloroethyl ethyl sulfide (**CEES**) and 2-chloroethyl phenyl sulfide (**CEPS**)) toward the corresponding sulfoxide **HDO** (**CEESO** or **CEPSO**) is by far the most represented in the literature. It is however critical to avoid overoxidation to the corresponding sulfones (**HDO**₂, **CEESO**₂ or **CEPSO**₂), the latter having acute toxicity as precursors of potentially strong electrophilic Michael acceptors (vinyl sulfone derivatives **CEVSO**₂, **EVSO**₂ or **PVSO**₂) (Fig. 1).

Among oxidative neutralization protocols, photocatalytic processes have attracted a lot of attention (Fig. 2a).^{5,18,30–41} Stoichiometric oxidizers are also reported, such as *N,N*-dichloroethane,⁴² yet they suffer from poor atom-economy.^{43,44} Extensive formation of α -monochlorinated sulfoxide (**HDOCl**), a neutralized form of **HD**, is often reported under these conditions.^{45,46} Other more typical oxidizers have been reported in combination with innovative process technologies. For instance, Legros *et al.* reported a series of continuous flow processes using stoichiometric oxidizers under homogeneous or heterogeneous conditions (Fig. 2b and c): (a) a first report in 2017 where the authors disclosed a continuous flow setup relying on the hydrogen peroxide/urea complex (UHP) as an oxidizer in methanol in the presence of methanesulfonic acid⁴⁷ and (b) a more recent report in 2021 relying on Oxone (2 KHSO₅ KHSO₄ K₂SO₄) in a packed-bed flow setup.² In both cases, the oxidation of **CEES** afforded selectively the corresponding sulfoxide **CEESO** with a complete conversion in less than 5 min.

The most common decontamination protocol used by Emergency Responders or Armed Forces relies on aqueous solutions of hypochlorites.⁴⁸ This common protocol suffers

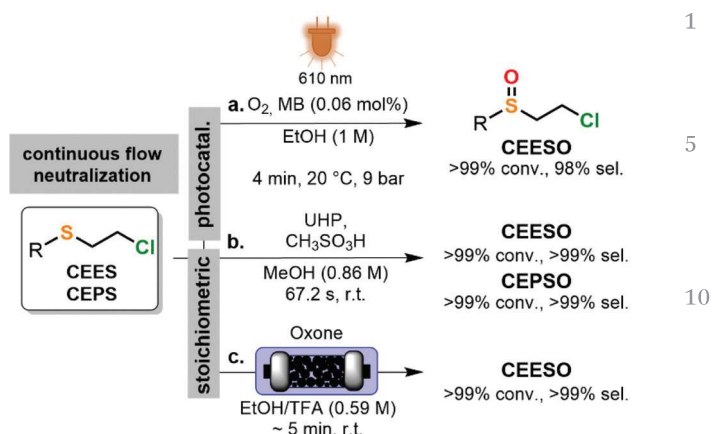


Fig. 2 Typical oxidative continuous flow protocols for the chemical neutralization of **HD** and its simulants. (a) Photocatalytic oxidation with singlet oxygen.⁵ (b) Stoichiometric oxidizer under homogeneous conditions.⁴⁷ (c) Stoichiometric oxidizer under heterogeneous conditions.²

from 4 major drawbacks: (a) the high lipophilicity of **HD** often leads to micelle formation/oligomerization and, hence, superficial oxidative neutralization of **HD** droplets;^{49–52} (b) the oxidation of **HD** (or simulants **CEES/CEPS**) with aqueous hypochlorites is a strongly exothermic reaction that generates quantities of overoxidized product (**HDO**₂, **CEESO**₂ or **CEPSO**₂, Fig. 1) and chlorinated sulfoxide products (such as **HDOCl**, **CEESOCl** or **CEPSOCl**, Fig. 1);⁵³ (c) the aggressive nature of bleach solution also raises significant corrosion issues in the decontamination of metal-based hardware and above all (d) the use of aqueous solutions leads to a huge quantity of polluted water that needs to be further retreated.

A solution was sought to address the most common issues associated with the oxidative neutralization of **HD** and its simulants (**CEES** and **CEPS**). An effective solution would rely on widely available reagents, a compact and safe setup amenable to large scales and an organic medium to ease the final downstream incineration. The use of lipophilic alkyl hypochlorites was envisioned to circumvent the high lipophilicity of **CEES** and **CEPS** and ensure their sulfoxidation with high selectivity. Specifically, **MeOCl**, **EtOCl**, **iPrOCl** and **tBuOCl** were explored under continuous flow conditions in order to (a) mitigate the relative instability of small organic hypochlorites^{54–69} and (b) ensure a precise control on the reaction conditions and selectivity.^{54–72}

To reach such ambition, we devised a continuous flow Chemical Generator of organic hypochlorites. The concept of Chemical Generators in flow, which was extensively documented by Kappe and coworkers,^{70–73} is summarized in Fig. 3a. It combines the main assets of flow technology with the inherent high reactivity of specific chemicals, providing robust, scalable, and safe protocols for exploiting such species at their fullest. Building upon our previous work on the generation of α -chloro-nitrosocycloalkyl species with **tBuOCl**,⁷⁴ a chemical generator for organic hypochlorites was devised. The generator was fed with widely available, stable, and low toxicity chemi-

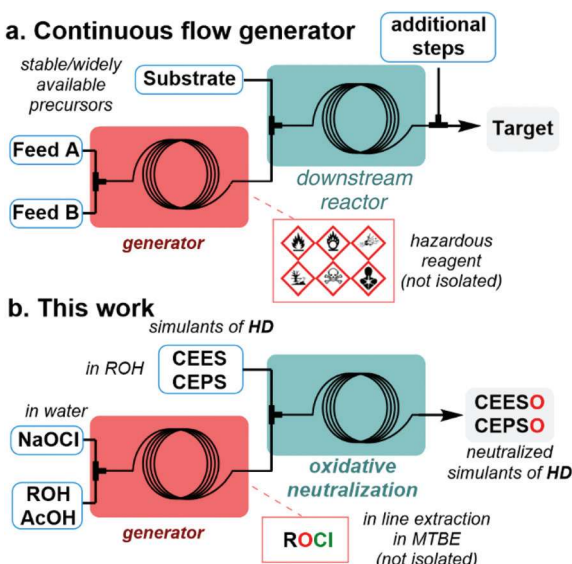


Fig. 3 (a) General concept of a chemical generator under continuous flow conditions. (b) This work: development of an upstream chemical generator for the safe preparation of discrete amounts of lower alkyl hypochlorous esters.

cals, including common lower alcohols (MeOH, EtOH, iPrOH, tBuOH), acetic acid and an aqueous solution of sodium hypochlorite (Fig. 3b). The corresponding lipophilic alkyl hypochlorites were then subjected to in-line membrane separation, providing an organic stream (MTBE) of hypochlorites directly usable for the sulfoxidation of **HD** simulants. Connecting the upstream generator to a downstream unit that immediately consumes organic hypochlorites significantly contributes to reducing operation and exposure hazards.

This work provides a thorough mechanistic investigation, combining experiments and computational chemistry, as well as an advanced optimization of the process conditions. We also document an *in silico* approach comparing computed reaction parameters on actual **HD** to extract reaction profiles to be compared with the experimental and computational data generated with its simulants. Such an approach offers insight into the potential transposition of model chemistries on an actual CWA, with minimal risks for the operator. The process was developed at the microfluidic scale and transposed to a mesofluidic commercial setup to validate its utilization at larger scales. This simple, yet elegant and robust protocol provides consistent neutralization with high selectivity while feeding upon simple, non-toxic, cheap, and widely available chemicals. The setup is engineered to possess a low footprint, which makes it a potential solution for rapid and efficient deployment.

Experimental section

General information

Conversion, selectivity, and yield were determined by gas chromatography coupled with Flame Ionization Detection

(GC-FID) or Mass Spectrometry (GC-MS) or by High Performance Liquid Chromatography coupled with Diode-Array Detection (HPLC-DAD) or Mass Spectrometry (LC-MS). Commercial standards or synthesized reference samples following reported procedures (see ESI, section 5† for experimental procedures) were used for LC and GC reaction monitoring. The selectivity toward the sulfoxide is defined as the ratio between the area% of the sulfoxide and the sum of the area% of all oxidation products. The neutralization selectivity is defined as the ratio between the sum of the area% of all sulfoxide derivatives (including the chlorinated sulfoxides) and the sum of the area% of all oxidation products. The neutralization selectivity is reported only for the most favorable cases. Structural identity was confirmed by ¹H and ¹³C NMR spectroscopy (400 MHz Bruker Avance spectrometer), by LC-MS or GC-MS (ESI, section 5†). Thioanisole (**1a**), methyl phenyl sulfoxide (**2a**), chloromethyl phenyl sulfoxide (**3a**), methyl phenyl sulfone (**6a**), chloromethyl phenyl sulfone (**7a**), diphenyl sulfide (**1b**), diphenyl sulfoxide (**2b**), diphenyl sulfone (**6b**), dibenzo[b,d]thiophene (**1c**), dibenzo[b,d]thiophene 5-oxide (**2c**), dibenzo[b,d]thiophene 5,5-dioxide (**6b**), dipropyl sulfide (**1d**), dipropyl sulfoxide (**2d**), dipropyl sulfone (**6d**), 2-chloroethyl ethyl sulfide (**CEES**), 2-chloroethyl phenyl sulfide (**CEPS**), methanol, ethanol, 2-propanol, *tert*-butanol, MTBE, acetic acid, and sodium hypochlorite pentahydrate were purchased from commercial sources and used without additional purification (ESI, section 2.1†). **CEESO**, **CEPSO** and **CEPSOCl** were prepared according to adapting protocols from the literature^{75,76} (ESI, section 5†).

CAUTION: 1-chloro-2-(ethylsulfinyl)ethane (**CEES**) and 2-chloroethyl phenyl sulfide (**CEPS**) are highly toxic and severe vesicants. Organic hypochlorites are heat-, light- and shock-sensitive materials and react violently with rubber. Methyl hypochlorite spontaneously and vigorously decomposes at room temperature. The isolation of **MeOCl**, **EtOCl** and **iPrOCl** should not be attempted. **tBuOCl** can be stored over CaCl_2 at 4 °C in a brown glass container for several days. Reactor setups involving organic hypochlorites were covered with aluminum foil to prevent light exposure. The concentration of organic hypochlorites was determined by back-titration. The reader should become aware of legal restrictions in their country on the permittance to study of **HD** or any related analogues of chemical warfare agents before possessing them in the lab.

Computations

Computations were performed at the B3LYP/6-311+G** level of theory with empirical dispersion (gd3bj) using the Gaussian 09 package of programs (Revision D.01) with implicit solvation (SMD, methanol).⁷⁷ Stationary points were optimized with gradient techniques (tight optimization convergence). Transition states were localized using the Newton-Raphson algorithm, and the nature of the stationary points was determined by analysis of the Hessian matrix. Intrinsic reaction coordinate (IRC) calculations were performed on representative transition states. Cartesian coordinates for representative stationary points are available in the ESI (section 6†).

Experimental setup

Microfluidic setups. Microfluidic setups were constructed from PFA tubing (1.58 mm outer diameter, 750 μm internal diameter) equipped with PEEK/ETFE connectors and ferrules (IDEX/Upchurch Scientific). Feed and collection lines consisted of PFA (1.58 mm outer diameter, 750 μm internal diameter) equipped with PEEK/ETFE connectors and ferrules (IDEX/Upchurch Scientific). Liquid feeds were handled with Chemyx Fusion 6000 syringe pumps (SS syringes equipped with DuPont Kalrez O-rings) or with HPLC pumps (Knauer Q4 Asurea equipped with a ceramic head). The temperature was regulated with a Heidolph MR Hei-Tec equipped with a Pt-1000 temperature sensor. Downstream pressure was regulated with back pressure regulators from Zaiput Flow Technologies (BPR-10) or from IDEX/Upchurch Scientific (BPR 75 psi). Liquid-liquid extraction was carried out with a Zaiput Flow Technologies membrane separator (SEP-10, equipped with a 1 μm pore hydrophobic membrane). See ESI, section 1.1 \dagger for details of the microfluidic setups.

Mesofluidic setup – lab scale. Lab scale mesofluidic experiments were carried out in a Corning® Advanced-Flow™ Lab Reactor (2.7 mL internal volume glass fluidic modules). Feed and collection lines consisted of PFA tubing (1/8" o.d.) with PFA or SS Swagelok connectors and ferrules. The process temperature was regulated with a LAUDA Integral XT 280 thermostat. See ESI, section 1.2 \dagger for details of the mesofluidic setup.

Continuous flow preparation of organic hypochlorites (microfluidic scale). The feed solution of sodium hypochlorite (1.5 M in water) and an aqueous solution of acetic acid and the alcohol precursor (1 M, 1/1 ratio) were both injected through a PEEK arrowhead micromixer at 0.1 mL min^{-1} and reacted in a PFA capillary coil for 5 min of residence time at 25 °C. MTBE was injected downstream (0.2 mL min^{-1}) through an additional PEEK T-mixer and the corresponding organic hypochlorite was extracted through a short column loaded with glass beads ($\phi = 0.1$ mm) coupled with a hydrophobic membrane separator. The concentration of the outgoing effluent was next assessed through iodometric back-titration.

Concatenation of the upstream *t*BuOCl generator with the downstream oxidation module (microfluidic scale). The feed solution of sodium hypochlorite (1.5 M in water) and an aqueous solution of acetic acid and *t*-butanol (1 M, 1/1 ratio) were both injected through a PEEK arrowhead micromixer at 0.1 mL min^{-1} and reacted in a PFA capillary coil for 5 min of residence time at 25 °C. MTBE was injected downstream (0.2 mL min^{-1}) through an additional PEEK T-mixer and *t*BuOCl was extracted through a short column loaded with glass beads ($\phi = 0.1$ mm) coupled with a hydrophobic membrane separator. The organic effluent (*t*BuOCl, 0.5 M in MTBE) was connected to a PEEK arrowhead micromixer where it was mixed with a solution of **1a** in MeOH (0.5 M, 0.2 mL min^{-1}) and reacted at 0 °C in a PFA coil (1.58 mm outer diameter, 750 μm internal diameter) for 60 s of residence time. The reactor effluent was diluted in acetonitrile and analyzed by LC-DAD.

Continuous flow oxidative neutralization of CEES and CEPS with *t*BuOCl (microfluidic scale). The feed solutions of CEES or CEPS diluted in MeOH (0.5 M) and *t*BuOCl diluted in MTBE (0.6 M for CEES and 0.7 M for CEPS) were both injected at 0.4 mL min^{-1} through a PEEK arrowhead micromixer and reacted in a PFA capillary coil for 60 s at 0 °C. The reactor effluent was diluted in acetonitrile and analyzed by GC-FID (CEES) or LC-DAD (CEPS).

Continuous flow oxidative neutralization of CEES and CEPS with *t*BuOCl (mesofluidic scale). A MTBE solution containing *t*BuOCl (0.6 M for CEES and 0.7 M for CEPS) was mixed and reacted with another feed solution containing either CEES or CEPS (0.5 M in MeOH) in a Corning® Advanced-flow™ Lab Reactor (2 glass fluidic modules connected in series, 5.4 mL total internal volume) operated at 0 °C. The flow rates were both set to 2.7 mL min^{-1} with an estimated residence time of 60 s for the neutralization of both CEES and CEPS. The reactor effluent was diluted in acetonitrile and analyzed by GC-FID (CEES) or LC-DAD (CEPS).

Results and discussion

The original protocol from Mintz and Walling was adapted for the preparation of a small library of hypochlorous esters. This process involves the reaction of a lower alcohol (MeOH, EtOH, iPrOH and *t*BuOH) in the presence of sodium hypochlorite and acetic acid in water (Fig. 5).⁷⁸ Preliminary trials in batch confirmed the near instantaneous reaction of hypochlorous acid with MeOH, EtOH, iPrOH and *t*BuOH, yielding a yellowish lipophilic phase of lower density than the aqueous reaction mixture. The extraction efficiency can be improved with an organic solvent (typically MTBE). The reaction was carried out at 0 °C for 30 minutes in the dark to avoid degradation of the corresponding hypochlorites (ESI, section 2.2.3 \dagger). The protocol was first optimized under batch conditions, and rapidly transposed to flow conditions after witnessing the spontaneous and vigorous decomposition of **MeOCl** and **EtOCl** upon extraction. NMR analysis on the crude hypochlorites revealed that the formation of *t*BuOCl was very selective, while the formation of **MeOCl**, **EtOCl** and **iPrOCl** came with a variety of side products.^{56–60}

The hypochlorite generator was constructed from PFA coils and HPLC-type connectors (ESI, section 1.4.1 \dagger) (Fig. 4). To avoid the collection of neat hypochlorites, the reactor effluent was connected to an additional T-mixer for a downstream extraction with an organic solvent. The flow rate of the extraction medium was adjusted to reach the desired concentration. The resulting segmented reaction mixture was next redirected to a membrane separator (hydrophobic PTFE membrane, 1 μm pore size). MTBE was selected as a preferential extraction medium for further experiments since it does not react with hypochlorites. The results of the iodide back titration emphasized the much lower stability of **MeOCl** compared to the other 3 organic hypochlorites. With theoretical concentrations of 1 M in MTBE, the titrations of **MeOCl**, **EtOCl**, **iPrOCl** and

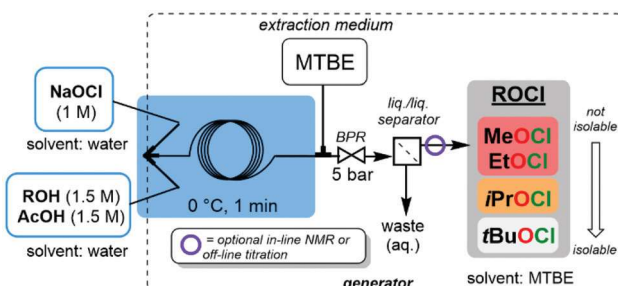


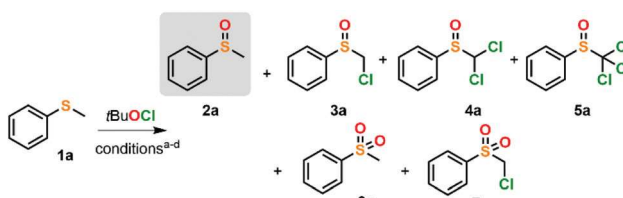
Fig. 4 Continuous flow generator of hypochlorous esters at the microfluidic scale (ESI, section 1.4.1†).

tBuOCl in MTBE gave 0.11, 0.96, 0.86 and 0.98 M, respectively (ESI, section 2.2.3†).

With the proof of concept of an upstream generator of organic hypochlorites in hand, the oxidation of model thioether compounds was next investigated. The selection of model thioethers included thioanisole (**1a**), diphenyl sulfide (**1b**), dibenzothiophene (**1c**) and dipropyl sulfide (**1d**). Compounds **1a–d** were used to calibrate the protocol and set boundaries, as well as to identify potential competitive reactions and side products. Compounds **1b,c** are known to be quite reluctant to well-described photocatalytic oxidations with singlet oxygen, while compounds **1a** and **1d** were validated as reliable, low toxicity simulants of **HD** in a recent publication.⁵ There is, however, an additional structural feature in **1a** and **1d**, which is lacking from **1b,c**, namely, protons at the α -position of the corresponding sulfoxides. The presence of mildly acidic protons ($pK_a \sim 33$ in DMSO for **2a**) at the α -position of the sulfoxide opens a competitive path, that is, the α -chlorination of the sulfoxide. With compound **1a**, the competitive chlorination can potentially yield the corresponding α -mono-chlorinated, α,α -bis-chlorinated and α,α,α -tris-chlorinated sulfoxides **3a**, **4a** and **5a**, respectively (Scheme 1).^{69,75,79–85}

Preliminary trials in batch were attempted with **tBuOCl** (ESI, section 3.1†). For the first set of reactions, the experiments involved reacting both a 0.5 M solution of **1a** and a 0.5 M solution of **tBuOCl** in MeOH (Scheme 1). However, the stock solution of **tBuOCl** in MeOH rapidly decomposed. An additional NMR study clearly showed the hypochlorite exchange between **tBuOCl** and MeOH, hence leading to the near-instantaneous formation of **MeOCl** that further decomposed (Fig. 5) (ESI, section 2.2.4†). Preliminary trials in batch were therefore attempted in MTBE.

A preliminary test reaction involving the oxidation of thioanisole (**1a**, 0.5 M in MTBE) under biphasic conditions with aqueous NaOCl·5H₂O at 0 °C led to a conversion of 58% and 87% selectivity to sulfoxide **2a** along with the formation of a significant amount of sulfone **6a** (10%) after 1 min of reaction. Next, the oxidation under homogeneous conditions with **tBuOCl** was investigated. Dropwise addition of neat **tBuOCl** (over 10 s, 1.1 equiv.) to a 15 mL solution of **1a** in MTBE (0.5 M) gave a near instantaneous conversion at 0 °C that plateaued



Conditions	2a	3a	4a	5a	6a	7a
a. MTBE	47 (31)	4	1	3 (6)	1	n.d.
b. MTBE w/10% MeOH	67 (64)	8 (9)	<1	n.d.	<1	n.d.
c. MTBE w/10% MeOH 1.1 equiv. pyridine	40 (29)	4 (5)	<1	2 (4)	<1	n.d.
d. MTBE w/10% MeOH 2 equiv. TEMPO	55 (58)	n.d.	n.d.	8	n.d.	

Scheme 1 Preliminary optimization in batch for the oxidation of thioanisole (**1a**) as a model compound (ESI, section 3.1†) with the distribution of products from the direct oxidation of **1a** with **tBuOCl** in MTBE or MTBE with MeOH (10%). The reaction was monitored by LC analysis at 200 nm; values are expressed in %area after 4 min of reaction (values in parentheses are for data collected after 40 min of reaction). n.d. = not detected. Conditions: (a) addition of neat **tBuOCl** (1.1 equiv.) over 10 s to 0.5 M solution of **1a** (in MTBE), 0 °C with reaction monitoring over 40 min, after which up to 22% of unidentified products were detected by LC; (b) addition of neat **tBuOCl** (1.1 equiv.) over 10 s to 0.5 M solution of **1a** (in MTBE with 10% MeOH), 0 °C with reaction monitoring over 40 min; (c) addition of neat **tBuOCl** over 10 s to 0.5 M solution of **1a** (in MTBE with 10% MeOH) and pyridine (1.1 equiv.), 0 °C with reaction monitoring over 40 min, after which up to 42% of unidentified products were detected by LC; (d) addition of neat **tBuOCl** over 10 s to 0.5 M solution of **1a** (in MTBE with 10% MeOH) and TEMPO (2 equiv.), 0 °C with reaction monitoring over 40 min, after which up to 16% of unidentified products were detected by LC.

at 69% after 4 min with a selectivity of 69% toward sulfoxide **2a** (Scheme 1). Besides trace amounts of α -mono-chlorinated sulfoxide **3a** (4%), α,α -bis-chlorinated sulfoxide **4a** (1%), α,α,α -tris-chlorinated sulfoxide **5a** (3%) and sulfone **6a** (1%), a large fraction of unidentified products (13%) was detected as well. The next set of experiments aimed at identifying the effect of MeOH on the oxidation reaction. A solution of model substrate **1a** (0.5 M, 15 mL) was prepared in MTBE with 10% MeOH and treated likewise with neat **tBuOCl** at 0 °C (Scheme 1). The reaction was again monitored, and the results differed quite significantly from the previous batch experiment. After complete addition of **tBuOCl**, the conversion plateaued at 77% with a selectivity of 88% toward sulfoxide **2a** with small amounts of **3a** (8%), traces of **4a** (<1%) and of sulfone **6a** (<1%); compound **5a** was not detected.

This preliminary set of observations thus suggested a very quick and selective oxidation of substrate **1a** with **tBuOCl** in the presence of MeOH and, most importantly, the formation of only trace amounts of sulfone **6a**. In conjunction with the rapid hypochlorite exchange reaction observed upon studying a solution of **tBuOCl** in MeOH (see above, Fig. 5), the higher conversion and cleaner reaction profile for the oxidation of **1a** in MTBE/MeOH strongly suggested that **MeOCl** was the term-

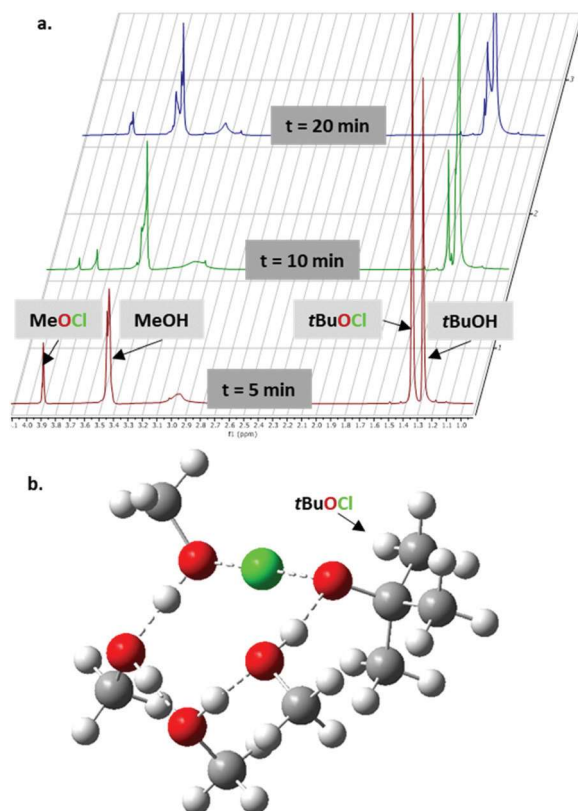
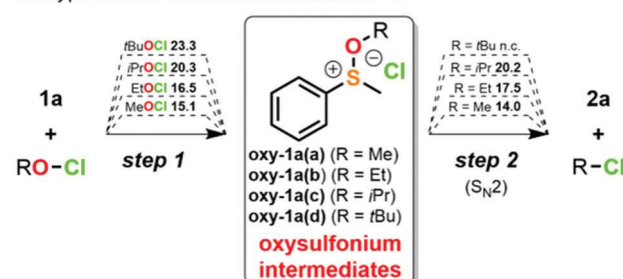


Fig. 5 Exchange of hypochlorites. (a) ^1H NMR monitoring of the hypochlorite exchange between tBuOCl and MeOH (CDCl_3). The first spectrum is recorded 5 min after the addition of tBuOCl and shows the formation of MeOCl and tBuOH ; after 10 min, MeOCl has almost completely decomposed and the amount of tBuOCl has decreased significantly; (b) tentative transition state for the hypochlorite exchange between tBuOCl and MeOH with a small cluster of MeOH (B3LYP/6-311+G***) (ESI, section 6.1†).

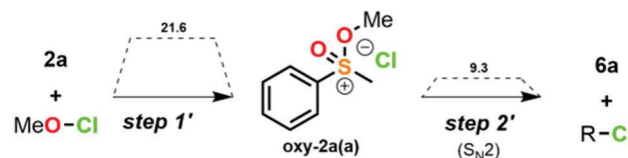
final oxidizer. These observations were supported with the computed activation barriers (see below, Fig. 6). An additional set of experiments was scheduled to gather more information on the mechanism and the species involved in the oxidation of **1a** (ESI, sections 3.1.3 & 3.1.4†). The formation of mono-chlorinated sulfoxides such as **3a** under similar conditions was documented in the literature,^{80,82,86} yet it involved the presence of a base (Scheme 1). However, when the reaction was performed in the presence of pyridine (1.1 equiv.) with **1a** in MTBE/MeOH (0.5 M, 10% MeOH), the conversion reached 80% with a 51% selectivity towards **2a** after 4 min with the significant formation of unidentified products (32%); surprisingly, the formation of α -chlorinated sulfoxides **3,4a** did not increase significantly (4 and <1%, respectively) in the presence of pyridine and remained stable over time; the formation of tris-chlorinated sulfoxide **5a** increased slightly over time (up to 4% after 40 min).⁶⁹

The likelihood of a homolytic mechanism was investigated by performing the oxidation of **1a** (0.5 M in MTBE with 10% MeOH) with tBuOCl in the presence of TEMPO, a well-described radical scavenger (Scheme 1) (ESI, section 3.1.4†).

a. Hypochlorite-mediated oxidation of **1a**



b. Overoxidation of **2a** toward **6a** (with MeOCl)



c. Snapshots of the TSs associated with steps 1, 1', 2 and 2'

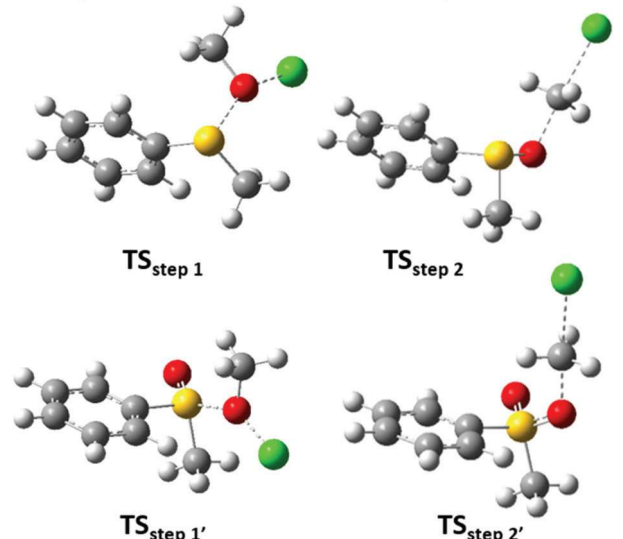


Fig. 6 Computational study for the oxidation and overoxidation of thioether with organic hypochlorites. (a) Computed reaction and activation enthalpies for selected model reactions (B3LYP/6-311+G**). Values are given in kcal mol^{-1} and computed in MeOH (n.c. = not computed). The oxidation toward sulfoxide **2a** and sulfone **6a** proceeds through a two-step mechanism: the preliminary formation of oxy sulfonium cationic intermediates (oxy-**1a,2a**) is followed with an $\text{S}_{\text{N}}2$ -type displacement with a chloride anion (ESI, section 6.1.2†). (b) Snapshots of the transition states corresponding to steps 1, 2 (oxidation to sulfoxide **2a**) and to steps 1', 2' (overoxidation to sulfone **6a**).

Under these conditions, the conversion toward **2a** plateaued at 80% with a selectivity of 70% which remained steady over 40 min of reaction monitoring. Interestingly, the formation of all chlorinated sulfoxides **3–5a** was suppressed, while the over-oxidation sulfone **6a** became the main side-product (8%). These results suggest that the formation of chlorinated sulfoxides **3–5a** most likely arises from a competitive radical-based mechanism. In the presence of TEMPO, the suppression of such a competitive path leaves a slight excess of tBuOCl , which

triggers the overoxidation of **1a** toward **6a** to a minor extent. An additional “competition” experiment with the oxidation of an equimolar mixture of **1a**, **2a** and **6a** further confirmed these hypotheses (ESI, section 3.2.8†).

The mechanism of sulfoxide formation in the presence of hypochlorites was thoroughly discussed by Ruff in 2011⁸⁷ and likely involves the formation of an oxysulfonium cationic intermediate (Fig. 6).⁸⁸ Computations were performed at the B3LYP/6-31+G** level of theory with the SMD model for the implicit inclusion of solvent for the reaction of **1a** with **MeOCl**, **EtOCl**, **iPrOCl** and **tBuOCl** (ESI, section 6.1†). The direct addition of the sulfur atom of **1a** onto the supposedly electrophilic Cl atom of the hypochlorites only gave an increasing enthalpy barrier without a transition state, while the addition on the O atom gave a transition state leading to the formation of an oxysulfonium cation intermediate **oxy-1a(a-d)** (Fig. 6).

The activation barrier towards **oxy-1a** increased with the steric hindrance of the starting hypochlorous esters: **oxy-1a(a)** ($R = Me$) $\Delta G^\ddagger = 15.1$ kcal mol⁻¹ < **oxy-1a(b)** ($R = Et$) $\Delta G^\ddagger = 16.5$ kcal mol⁻¹ < **oxy-1a(c)** ($R = iPr$) $\Delta G^\ddagger = 20.3$ kcal mol⁻¹ < **oxy-1a(d)** ($R = tBu$) $\Delta G^\ddagger = 23.3$ kcal mol⁻¹. The first step appeared exergonic (-18.4 kcal mol⁻¹ < $\Delta G^\circ < -21.2$ kcal mol⁻¹).

The second step involved the nucleophilic displacement of the electrophilic alkyl moiety of **oxy-1a(a-d)** with the chloride anion that was previously expelled. While an S_N2 mechanism is foreseen for **oxy-1a(a,b)**, a competition may occur for **oxy-1a(c)** and an S_N1 process is expected for **oxy-1a(d)**. It goes without saying that the corresponding enthalpy barriers are expected to follow the same order, the smallest one being associated with the S_N2 reaction on **oxy-1a(a)** ($\Delta G^\ddagger = 14.0$ kcal mol⁻¹), yielding sulfoxide **2a** and methylchloride (Fig. 6). Step 2 appeared mostly isoenergetic to step 1 regarding the activation barriers. The overoxidation toward the formation of sulfone **6a** is expected to follow the same pattern, with the intermediate formation of an oxysulfonium intermediate **oxy-2a**, followed by an S_N2 displacement. The overoxidation path was computed likewise for **2a** with **MeOCl** only. The formation of **oxy-2a** from sulfoxide **2a** was associated with an activation barrier of $\Delta G^\ddagger = 21.6$ kcal mol⁻¹ and a comparable exergonicity as for the formation of **oxy-1a** ($\Delta G^\circ = -20.1$ kcal mol⁻¹). The second step, namely, the S_N2 displacement with the chloride anion was associated with a much smaller activation barrier ($\Delta G^\ddagger = 9.3$ kcal mol⁻¹) and a strong exergonicity ($\Delta G^\circ = -22.7$ kcal mol⁻¹) both of which reflect the much higher electrophilicity of **oxy-2a** vs. **oxy-1a** and its better leaving group ability (Fig. 6). These results emphasize that it is unclear whether step 1 or step 2 is rate-determining for the formation of the sulfoxide, while for the overoxidation toward **6a**, it is clear that step 1' leading to oxysulfonium intermediate **oxy-2a(a)** is rate-determining. The computations however emphasized that step 1' leading to the overoxidation intermediate **oxy-2a(a)** comes with a much higher activation barrier than step 1 leading to **oxy-1a(a)** ($\Delta\Delta G^\ddagger = 6.5$ kcal mol⁻¹) (Fig. 6), which explains the full selectivity toward the sulfoxide organic hypochlorites.

Regarding the sulfoxidation step, a much lower activation barrier for the rate-determining step is obtained with **MeOCl** (15.1 kcal mol⁻¹), hence pointing toward its selection as a potent oxidizer. The observed instability for **MeOCl**, however, precludes its generation upstream despite its potential as a sulfoxidation reagent. The computed activation barriers agree with the hypothetic formation of much more reactive **MeOCl** upon mixing a stock solution of **1a** in MeOH and of **tBuOCl** in MTBE (see above). This opportunity was therefore envisioned as a robust and straightforward compromise between the stability combined with a lower sulfoxidation activity for **tBuOCl** and the instability of **MeOCl** with its superior ability to produce sulfoxides. The computations, however, clearly indicate that the likelihood of overoxidation towards **6a** should be minimized under these conditions.

With the combined insights from the preliminary batch trials and the computations, the oxidation of model **1a** was next attempted under continuous conditions (Fig. 7): (a) a high-performance micromixer was selected to reach rapid homogenization and hence potentially control the formation of competitive radical-based chlorination mechanisms and (b) **tBuOCl** was selected as a primary hypochlorous ester and was solubilized in MTBE to avoid decomposition in the feed, in conjunction with substrate **1a** in MeOH to take advantage of the *in situ* formation of more reactive **MeOCl**. The flow rates were set to have a 1:1.1 **1a/tBuOCl** ratio. The conditions were further optimized to assess the effects of the residence time, the mixing efficiency, the temperature, the excess **tBuOCl**, and the concentration and the nature of the alcohol additive (MeOH, EtOH, iPrOH and *t*BuOH) (ESI, section 3.2†).

The temperature was the first parameter evaluated, starting with standard operating conditions with 10 s residence time and a 1:1.1 **1a/tBuOCl**. At -78 °C, the conversion dropped significantly to 45% (>99% selectivity); raising the temperature to 20 °C increased the conversion to 80% with a selectivity of 98%, hence pointing 0 °C as the best compromise ensuring short residence time with high conversion (93%) and selectivity (99%) toward **2a**. The effects of both the excess **tBuOCl** and the concentration were next addressed. As expected, a substoichiometric amount (0.75 equiv.) of the oxidizer led to a much lower conversion (62%) while maintaining an excellent selectivity (98%); by contrast, a larger excess (2.1 equiv.) of oxidizer gave a quantitative conversion but a very low selectivity (30%) with the emergence of sulfone **6a**, the α -chlorinated sulfoxide **3a** and α,α -bis-chlorinated sulfoxide **4a** in significant amounts (6, 25 and 38%, respectively). Despite a lower selectivity toward **2a**, the neutralization selectivity, which includes all sulfoxide products, was still excellent (94%). The concentration also had a significant impact. With 0.5 M for both feeds, a conversion of 99% was reached within 60 s at 0 °C (91% selectivity, 99% neutralization selectivity). Increasing progressively the concentration to 2 M for both feeds led to a decreased conversion (81%) and selectivity (49%) with the formation of significant amounts of sulfone **6a**, α -mono-chlorinated and α,α -bis-chlorinated sulfoxides **3,4a** (2, 15 and 15%, respectively).

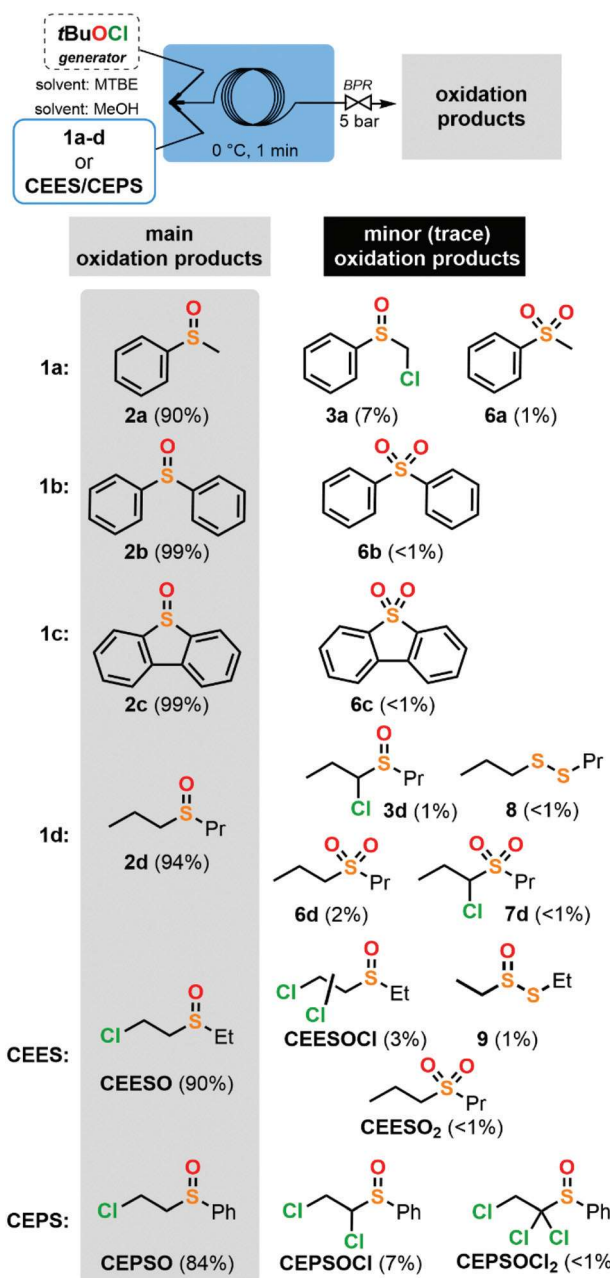


Fig. 7 Microfluidic setup for the hypochlorite-mediated oxidation of model thioethers **1–4a**, CEES and CEPS with the upstream generator of **tBuOCl**. Data from LC analysis (200 nm, for the oxidation on compounds **1a–c** and CEPS) or from GC-MS analysis (oxidation on compounds **1d** and CEES) on the crude reactor effluents using optimized conditions: 60 s of residence time, 0 °C with a 1 : 1.1 **1a**/**tBuOCl** unless otherwise stated in the main text. Feed solutions of **1a,b,d** CEES and CEPS were prepared in MeOH (0.5 M). Feed solution of **1c** was prepared in 50 : 50 MeOH/CH₂Cl₂ (0.25 M).

Despite a lower output, the concentration was therefore set at 0.5 M for the subsequent optimizations.

The next experiments addressed the effect of the residence and the mixing efficiency. The effect of the residence time was assessed at constant flow rates for both feeds by adjusting the

internal volume of the coil reactor. Three residence times (10, 30 and 60 s) were considered at 0 °C. The shortest residence time provided a conversion of 93% with a 99% selectivity towards sulfoxide **2a** with trace amounts of sulfone **6a** (<1%) and α -chlorinated sulfoxide **3a** (1%). Increasing the residence time to 30 s pushed the conversion to >99%, while the selectivity toward **2a** slightly decreased to 91%. In the latter, sulfone **6a** remained barely detectable (<1%), while the amount of **3a** increased significantly (8%). For the longest residence time (60 s), both conversion and selectivity remained unaffected. These preliminary microfluidic results emphasized once more the near-instantaneous and selective oxidation of **1a** toward **2a** and the control of the residence time appeared as an important parameter to minimize the competitive radical chlorination of **2a** and the overoxidation to **6a**. In the next set of experiments, the impact of the mixing efficiency was evaluated through experiments carried out in the same PFA coil with decreasing flow rates for both feeds with a constant 1 : 1.1 **1a**/**tBuOCl** ratio at 0 °C.

With the reference reaction at 10 s of residence time in mind (93% conversion, >99% selectivity), progressively degrading the mixing efficiency had a deleterious impact on both the conversion and the selectivity: 82% conversion and 98% selectivity were achieved within 30 s of residence time, while the experiment at 60 s gave 72% conversion and 84% selectivity (99% neutralization selectivity).

In conjunction with the preliminary batch trials, these results emphasize that poor mixing efficiency affects the output of the oxidation reaction. It is expected that longer residence times (not tested) associated with a poor mixing efficiency would lead to increasing impurities associated with a local excess of **tBuOCl** (presumably chlorinated derivatives: sulfoxides **3–5a** and sulfone **6a**). The last parameter that required some further preliminary trials concerned the selection of the alcohol used as the solvent for substrate **1a**. Though the main idea was to combine both the stability of **tBuOCl** with the high reactivity of **MeOCl** through an *in situ* generation of the latter from MeOH, 3 additional experiments were designed with incremental lower alcohols as solvents for **1a**. Under comparable conditions as for the MeOH/MTBE system (1.1 equiv. **tBuOCl**, 0 °C, 60 s), a lower conversion of 63% (39% selectivity) was obtained with EtOH as the solvent for **1a**. With isopropanol, the conversion went back to the upper 80 s (87%) with 74% selectivity (84% neutralization selectivity). Lastly, **tBuOH** led to 65% conversion and 62% selectivity (83% neutralization selectivity). In all 3 cases, sulfone **6a** was formed in about 5%, **3,4a** ranged from 10 to 27% and from 1 to 6%, respectively. To conclude this section, the best compromise to balance conversion and selectivity while forming minimal amounts of sulfone **6a** involves reacting 0.5 M feed solutions (thioanisole in MeOH and **tBuOCl** in MTBE), with a 1 : 1.1 stoichiometric ratio at 0 °C within 60 s of residence time with a high-performance arrow-head micro-mixer to reach complete conversion and very high selectivity (91%) and excellent neutralization selectivity (99%). Under these conditions, α -chlorinated sulfoxide **3a** becomes the

major side product (7%) and sulfone **6a** remains barely detectable (1%).

The feed of thioether was next changed to diphenylsulfide (**1b**) and dibenzothiophene (**1c**), both in solution in MeOH (Fig. 7). *tBuOCl* was generated upstream as a 0.5 M solution in MTBE. With substrates **1b,c**, which lack a proton at the alpha position, the formation of chlorinated sulfoxides does not compete with the oxidation or the overoxidation. With **1b**, total conversion was obtained under the same conditions. The corresponding sulfone **6b** was barely detected (<1%). With **1b**, the concentration had a limited impact on the reaction since complete conversion was maintained with 1 M concentration for each feed solution (99% selectivity). Decreasing the residence time to 30 s had a minor effect on the conversion (97%), while the selectivity remained unchanged (99%). Dibenzothiophene (**1c**) was poorly soluble in MeOH, and the corresponding feed solution was prepared in a 50 : 50 MeOH/CH₂Cl₂ blend (0.25 M). **1c** is notoriously difficult to oxidize; it was therefore not surprising that a larger excess of *tBuOCl* was required to reach complete conversion. A slight increase of the excess oxidant (1.2 equiv.) gave 99% conversion with a 98% selectivity.

The optimized conditions (1.1 equiv.) were next transposed to dipropyl sulfide (**1d**) (Fig. 7 and 8, and ESI, section 4.3†). Transposition on **1d** gave 98% conversion with 96% selectivity toward **2d** (97% neutralization selectivity), with a small amount of the corresponding sulfone (**6d**, 2%), and traces of the corresponding α -chlorinated sulfone **7d** (<1%) and the α -chlorinated sulfoxide **3d** (1%). 1,2-Dipropyldisulfane (**8**) was also detected in traces (<1%, see also Fig. 9b).⁸⁹ Slightly increasing the excess of *tBuOCl* to 1.2 equiv. slightly improved the conversion (98%), yet it produced more sulfone **6d** (5%) and its chlorinated analog **7d** (1%) with an overall neutralization selectivity of 94%.

Oxidative neutralization was then attempted on **CEES** and **CEPS** (Fig. 7). The conditions with 1.1 equiv. *tBuOCl* with **CEES** provided excellent conversion of 94% with a selectivity of 95% toward **CEESO** (neutralization selectivity of 97%) after 60 s of residence time at 0 °C. Sulfone **CEESO₂** and its chlorinated derivatives were barely detected (<1%). Other minor impurities included α -chlorinated sulfoxide **CEESOCl** (1%) and diethylsulfinate **9** (<1%, see Fig. 9b).^{90–92} Increasing the excess of *tBuOCl* to 1.2 equiv. led to 98% conversion with 92% selectivity toward **CEESO** (neutralization selectivity of 99%). Despite the slight excess of *tBuOCl* in the last trial, both **CEESO₂** and its chlorinated analog **CEESO₂Cl** remained barely detected, while diethylsulfinate **9** slightly increased (1%). With **CEPS**, 93% conversion was achieved with 90% selectivity towards **CEPSO** (98% neutralization selectivity). Sulfone **CEPSO₂** was not detected. Increasing the excess *tBuOCl* to 2 equiv. pushed the conversion to 98% but the selectivity towards **CEPSO** dropped to 16%, with major side-products including the mono- and bis-chlorinated sulfoxides **CEPSOCl** and **CEPSOCl₂** in 73% and 10%, respectively. Sulfone **CEPSO₂** remained undetected, despite the larger excess of *tBuOCl*.

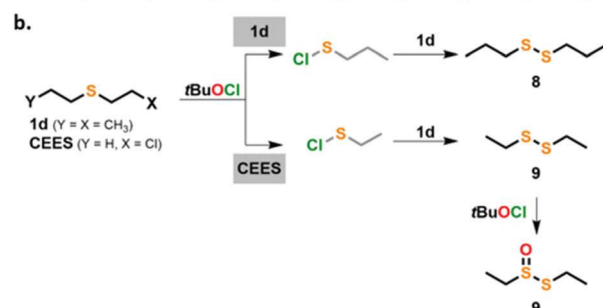
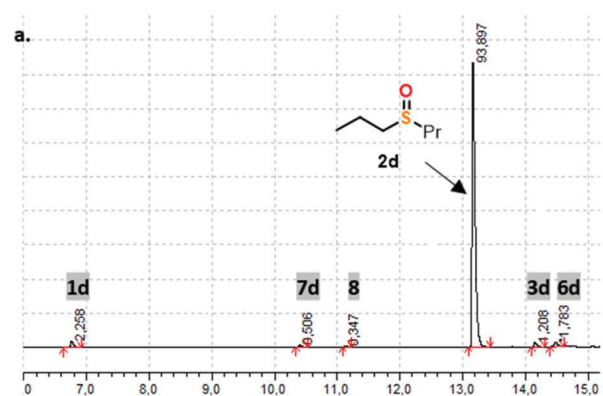


Fig. 8 (a) Typical GC chromatogram for the oxidation of **1d** (dipropyl sulfide), featuring the distribution of side-products. The attribution of peaks was carried out with the injection of commercial or synthesized reference samples (**1d**, **2d** and **6d**) or by GC-MS with NIST identification (**3d**, **7d** and **8**). (b) Tentative mechanism for the formation of impurities **8** and **9**.¹⁰³

The final stage of this study concerns the transposition of the best conditions for the oxidative neutralization of **CEES** from the microfluidic scale toward the mesofluidic scale (for **CEPS**, see ESI, section 4.8†). We used a commercial mesofluidic glass reactor setup (Corning® Advanced-Flow™ LF/G1 skid Reactor equipped with 2 glass fluidic modules connected in series (2.7 mL internal volume each, Fig. 9a). To simplify the setup, the upstream generator was disconnected from the downstream oxidation module. A fresh solution of *tBuOCl*, the molarity of which was controlled by back-titration, was used for the trials on **CEES** and **CEPS**. Full concatenation of a similar process was demonstrated elsewhere.⁷⁰ With a 60 s residence time at 0 °C, the oxidation of **CEES** reached 99% conversion with a 96% selectivity toward **CEESO**. The major impurity became mono-chlorinated sulfoxide **CEESOCl**, while sulfone **CEESO₂** remained undetected, hence providing a neutralization selectivity of 99% with a space time yield = 3.74 kg L⁻¹ h⁻¹.

Lastly, the oxidation of **HD** with **MeOCl** was computed and compared to the computational results associated with **CEES** to further validate *in silico* the potential transposition of this oxidative neutralization protocol to an actual CWA (Fig. 9b). Both the simulant and the actual **HD** came up with very close reaction profiles and activation barriers for the various steps leading to the corresponding sulfoxides and sulfones, hence suggesting that the experimental results for the neutralization

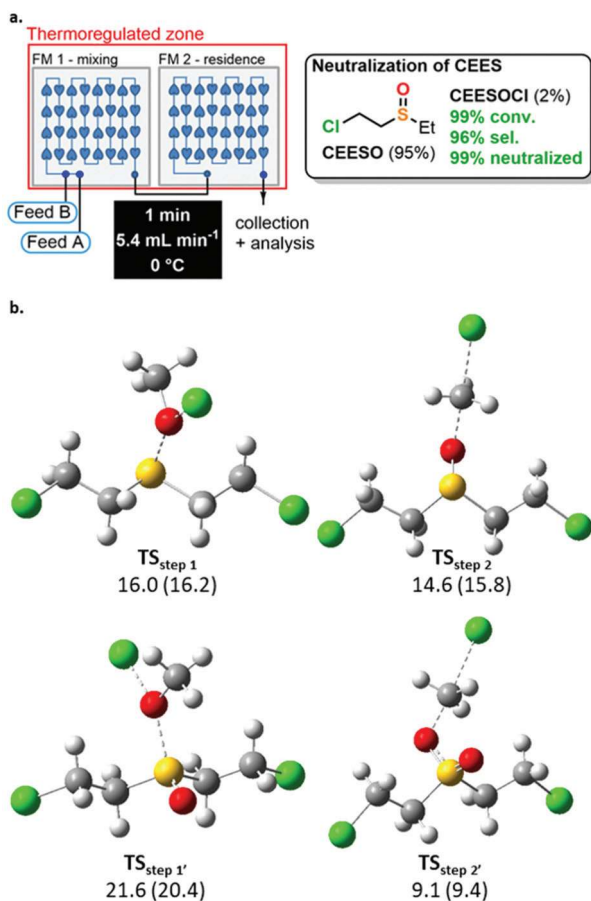


Fig. 9 (a) Mesofluidic reactor setup for the scalability trials featuring a Corning® Advanced-Flow™ LF/G1 skid Reactor equipped with 2 glass fluidic modules connected in series. Data from GC-MS (CEES) (b) transition state structures (B3LYP/6-311+G**) and activation energies (in kcal mol⁻¹) for the *in silico* oxidation of HD. Values in parentheses are calculated for CEES (ESI, sections 6.2 & 6.3†). See also Fig. 7 for details on the various steps.

of CEES are representative of the behavior of HD under similar experimental oxidative conditions (ESI, section 6.3†).

Conclusion

This work reports a scalable and robust continuous flow process for the oxidative neutralization of organosulfur CWA simulants. The process proposes an original solution to both produce and mitigate the high reactivity of lower alkyl hypochlorites from aqueous solutions of sodium hypochlorite. An upstream generator of organic hypochlorites produces a homogeneous stream of organic hypochlorites in MTBE that is further used downstream for the selective oxidation of thioethers. Despite the higher computed reactivity of **MeOCl** for the oxidation of thioethers to the corresponding sulfoxides, its inherent instability precludes its formation in the upstream generator. Instead, the upstream generation of **tBuOCl**, which is much more stable than **MeOCl**, but also much less reactive,

is advantageously exploited to feed the downstream oxidation module. The latter is fed with the thioether substrate in MeOH, which provokes a near-instantaneous hypochlorite exchange with MeOH hence producing “on-the-spot” **MeOCl**.

Such a strategy exploits the higher reactivity of **MeOCl** without the safety and reproducibility issues related to its instability. It provides convenient and fast oxidative conditions for the transformation of thioethers into their corresponding sulfoxides. There are, however, several competitive reactions: (a) a radical-based chlorination of the sulfoxide, typically leading to their corresponding α -chlorinated derivatives (sometimes multiple chlorinations are observed); (b) the formation of disulfides or sulfinites through an intermediate sulfenyl chloride and (c) an overoxidation to the corresponding sulfone. While competitive paths (a) and (b) are not concerning when it comes to the efficiency of the oxidative neutralization (since they may be considered as neutralized species), the emergence of a competitive overoxidation is more concerning. Fortunately, in all trials executed in this study, the formation of the overoxidation sulfone is usually <1%. The use of organic hypochlorites alleviates the formation of micelles and superficial chemical neutralization of sulfur mustards with aqueous hypochlorites. The preliminary transformation of aqueous sodium hypochlorite into the corresponding lower alkyl hypochlorous esters remains accessible according to a straightforward protocol that accommodates either batch (for the most stable hypochlorites such as **tBuOCl**) or flow procedures. The conditions were optimized on model thioethers and then adapted for the neutralization of CEES and CEPS, both under microfluidic and mesofluidic conditions, with excellent conversion and neutralization selectivity. The process relies on widely accessible and affordable chemicals and is amenable to larger scales for the chemical neutralization of large inventories of sulfur mustard vesicants to low-toxicity sulfoxides, which can thereafter be safely transported to incineration facilities. The flexibility (simple chemicals, liquid feeds and liquid wastes) and efficiency (space time yield = 3.74 kg L⁻¹ h⁻¹) of this new system outclass other recently reported neutralization protocols of CEES under flow conditions (with singlet oxygen:⁵ STY = 0.58 kg L⁻¹ h⁻¹ and with oxone:² STY = 0.31 kg L⁻¹ h⁻¹). Besides the pragmatic aspects of this process, computational chemistry is used here as a convenient way to explore the pertinence of the protocols developed on simulants for the neutralization of HD, hence providing indication of potential transposition toward actual sulfur CWAs without military clearance and without extremely restrictive safety protocols.

Conflicts of interest

There are no conflicts to declare.

Acknowledgements

This work was supported by the F.R.S.-FNRS. Computational resources were provided by the “Consortium des Équipements

1 de Calcul Intensif" (CÉCI), funded by the "Fonds de la
2 Recherche Scientifique de Belgique" (F.R.S.-FNRS) under Grant
3 No. 2.5020.11. VEK holds a F.R.S.-FNRS FRIA PhD fellowship
4 (grant no. FC27539). DVSB acknowledges NASA EPSCoR for
5 funding (Personalized Medication System for Deep Space
6 Missions, NASA grant 80NSSC19M0148). The authors thank
7 Dr Morgan Hans for the access to the GC-MS facility.
8 Dr Guillaume Gauron and Alessandra Vizza (Corning SAS) are
9 acknowledged for the loan of the AFR reactors, technical and
10 scientific support for the scalability trials.

15 Notes and references

- 1 S. Balasubramanian, A. J. Kulandaivelu, K. J. Babu, A. Das and J. B. Balaguru Rayappan, *Ind. Eng. Chem. Res.*, 2021, **60**, 4218–4239.
- 2 A. Delaune, S. Mansour, B. Picard, P. Carrasqueira, I. Chataigner, L. Jean, P.-Y. Renard, J.-C. M. Monbaliu and J. Legros, *Green Chem.*, 2021, **23**, 2925–2930.
- 3 P. A. DeSario, W. O. Gordon, A. Balboa, A. M. Pennington, C. L. Pitman, M. McEntee and J. J. Pietron, *ACS Appl. Mater. Interfaces*, 2021, **13**, 12550–12561.
- 4 A. M. Ebrahim, A. M. Plonka, Y. Tian, S. D. Senanayake, W. O. Gordon, A. Balboa, H. Wang, D. L. Collins-Wildman, C. L. Hill, D. G. Musaev, J. R. Morris, D. Troya and A. I. Frenkel, *ACS Appl. Mater. Interfaces*, 2020, **12**, 14721–14738.
- 5 N. Emmanuel, P. Bianchi, J. Legros and J.-C. M. Monbaliu, *Green Chem.*, 2020, **22**, 4105–4115.
- 6 Y. Kalinovskyy, A. J. Wright, J. R. Hiscock, T. D. Watts, R. L. Williams, N. J. Cooper, M. J. Main, S. J. Holder and B. A. Blight, *ACS Appl. Mater. Interfaces*, 2020, **12**, 8634–8641.
- 7 S. Mansour, A. Delaune, M. Manneveau, B. Picard, A. Claudel, C. Vallières, L. Sigot, P.-Y. Renard and J. Legros, *Green Chem.*, 2021, **23**, 7522–7527.
- 8 M. L. Mendonca, D. Ray, C. J. Cramer and R. Q. Snurr, *ACS Appl. Mater. Interfaces*, 2020, **12**, 35657–35675.
- 9 B. Picard, I. Chataigner, J. Maddaluno and J. Legros, *Org. Biomol. Chem.*, 2019, **17**, 6528–6537.
- 10 O. Redy Keisar, V. Nahum, L. Yehezkel, I. Marcovitch, I. Columbus, G. Fridkin and R. Chen, *ACS Omega*, 2021, **6**, 5359–5367.
- 11 G. Thomas and D. Spitzer, *ACS Appl. Mater. Interfaces*, 2021, **13**, 47185–47197.
- 12 N. Tuccitto, L. Riela, A. Zammataro, L. Spitaleri, G. Li-Destri, G. Sfuria, G. Nicotra, A. Pappalardo, G. Capizzi and G. Trusso Sfrazzetto, *ACS Appl. Nano Mater.*, 2020, **3**, 8182–8191.
- 13 C. A. Valdez, R. N. Leif, S. Hok and B. R. Hart, *Rev. Anal. Chem.*, 2018, **37**.
- 14 A. Zammataro, R. Santonocito, A. Pappalardo and G. Trusso Sfrazzetto, *Catalysts*, 2020, **10**, 881.
- 15 X. Zhang, Y. Sun, Y. Liu, Z. Zhai, S. Guo, L. Peng, Y. Qin and C. Li, *ACS Appl. Mater. Interfaces*, 2021, **13**, 39976–39984.
- 16 C. R. Jabbour, L. A. Parker, E. M. Hutter and B. M. Weckhuysen, *Nat. Rev. Chem.*, 2021, **5**, 370–387.
- 17 J. Nawała, P. Jóźwik and S. Popiel, *Int. J. Environ. Sci. Technol.*, 2019, **16**, 3899–3912.
- 18 E. Oheix, E. Gravel and E. Doris, *Chem. – Eur. J.*, 2021, **27**, 54–68.
- 19 <https://www.un.org/disarmament/wmd/chemical/>, (accessed October 26th 2021).
- 20 <https://www.opcw.org/our-work/what-chemical-weapon>, (accessed October 26th 2021).
- 21 <https://www.iss.europa.eu/sites/default/files/EUSSIFiles/Brief%2017%20Chemical%20weapons.pdf>, (accessed 26th October 2021).
- 22 K. Ma, M. C. Wasson, X. Wang, X. Zhang, K. B. Idrees, Z. Chen, Y. Wu, S.-J. Lee, R. Cao, Y. Chen, L. Yang, F. A. Son, T. Islamoglu, G. W. Peterson, J. J. Mahle and O. K. Farha, *Chem. Catal.*, 2021, **1**, 721–733.
- 23 E. Mahayoni, S. Min, J. Kim, K. Jeong and S. H. Kim, *J. Hazard. Mater.*, 2021, **411**, 125144.
- 24 H. Prihed, A. Shifrovich, T. Shamai Yamin, M. Madmon, B. Smolkin, R. Chen, M. Blanca and A. Weissberg, *J. Mass Spectrom.*, 2021, **56**, e4721.
- 25 P. Vanninen, A. Östlin, J. Beldowski, E. A. Pedersen, M. Söderström, M. Szubskia, M. Grabowski, G. Siedlewicz, M. Czub, S. Popiel, J. Nawała, D. Dziedzic, J. Jakacki and B. Paćzek, *Mar. Environ. Res.*, 2020, **161**, 105112.
- 26 Y. J. Jang, K. Kim, O. G. Tsay, D. A. Atwood and D. G. Churchill, *Chem. Rev.*, 2015, **115**, PR1–PR76.
- 27 F. N. Diauudin, J. I. A. Rashid, V. F. Knight, W. M. Z. Wan Yunus, K. K. Ong, N. A. M. Kasim, N. Abdul Halim and S. A. M. Noor, *Sens. Bio-Sens. Res.*, 2019, **26**, 100305.
- 28 Y. Wu, J. Dong, C. Liu, X. Jing, H. Liu, Y. Guo, Y. Chi and C. Hu, *Dalton Trans.*, 2021, **50**, 9796–9803.
- 29 B. A. Lagasse, L. McCann, T. Kidwell, M. S. Blais and C. D. Garcia, *ACS Omega*, 2020, **5**, 20051–20061.
- 30 Y. Liu, C. T. Buru, A. J. Howarth, J. J. Mahle, J. H. Buchanan, J. B. DeCoste, J. T. Hupp and O. K. Farha, *J. Mater. Chem. A*, 2016, **4**, 13809–13813.
- 31 C. T. Buru, M. B. Majewski, A. J. Howarth, R. H. Lavroff, C.-W. Kung, A. W. Peters, S. Goswami and O. K. Farha, *ACS Appl. Mater. Interfaces*, 2018, **10**, 23802–23806.
- 32 A. J. Howarth, C. T. Buru, Y. Liu, A. M. Ploskonka, K. J. Hartlieb, M. McEntee, J. J. Mahle, J. H. Buchanan, E. M. Durke, S. S. Al-Juaid, J. F. Stoddart, J. B. DeCoste, J. T. Hupp and O. K. Farha, *Chem. – Eur. J.*, 2017, **23**, 214–218.
- 33 H. Wang, G. W. Wagner, A. X. Lu, D. L. Nguyen, J. H. Buchanan, P. M. McNutt and C. J. Karwacki, *ACS Appl. Mater. Interfaces*, 2018, **10**, 18771–18777.
- 34 D. Cambié, C. Bottecchia, N. J. W. Straathof, V. Hessel and T. Noël, *Chem. Rev.*, 2016, **116**, 10276–10341.
- 35 K. Donnelly and M. Baumann, *J. Flow Chem.*, 2021, **11**, 223–241.

1 36 C. Sambiagio and T. Noël, *Trends Chem.*, 2020, **2**, 92–106.

2 37 L. Buglioni, F. Raymenants, A. Slattery, S. D. A. Zondag and T. Noël, *Chem. Rev.*, 2022, **122**, 2752–2906.

3 38 J. D. Williams and C. O. Kappe, *Curr. Opin. Green Sustain. Chem.*, 2020, **25**, 100351.

4 39 A. Steiner, P. M. C. Roth, F. J. Strauss, G. Gauron, G. Tekautz, M. Winter, J. D. Williams and C. O. Kappe, *Org. Process Res. Dev.*, 2020, **24**, 2208–2216.

5 40 J. D. Williams, M. Nakano, R. Gérardy, J. A. Rincón, Ó. de Frutos, C. Mateos, J.-C. M. Monbaliu and C. O. Kappe, *Org. Process Res. Dev.*, 2019, **23**, 78–87.

10 41 T. Noël, *J. Flow Chem.*, 2017, **7**, 87–93.

15 42 P. K. Gutch, A. Mazumder and G. Raviraju, *RSC Adv.*, 2016, **6**, 2295–2301.

20 43 R. Singh, P. K. Gutch and A. Mazumder, *Ind. Eng. Chem. Res.*, 2013, **52**, 4689–4694.

25 44 P. K. Gutch and A. Mazumder, *Ind. Eng. Chem. Res.*, 2012, **51**, 5830–5837.

30 45 B. Smolkin, N. Levi, N. Karton-Lifshin, L. Yehezkel, Y. Zafrani and I. Columbus, *J. Org. Chem.*, 2018, **83**, 13949–13955.

35 46 N. Karton-Lifshin, S. Katalan, I. Columbus, R. Chen, L. Yehezkel, M. Madmon, S. Dagan, S. Elias, G. Fridkin and Y. Zafrani, *Chem. Commun.*, 2019, **55**, 12471–12474.

40 47 B. Picard, B. Gouilleux, T. Lebleu, J. Maddaluno, I. Chataigner, M. Penhoat, F.-X. Felpin, P. Giraudeau and J. Legros, *Angew. Chem., Int. Ed.*, 2017, **56**, 7568–7572.

45 48 D. H. Rosenblatt, M. J. Small, T. A. Kimmell and A. W. Anderson, *Background chemistry for chemical warfare agents and decontamination processes in support of delisting waste streams at the U.S. Army Dugway Proving Ground, Utah*, D. o. Defense, UNT Libraries Government Documents United States, Illinois.

50 49 F. M. Menger and M. J. Rourk, *Langmuir*, 1999, **15**, 309–313.

55 50 F. Gonzaga, E. Perez, I. Rico-Lattes and A. Lattes, *New J. Chem.*, 2001, **25**, 151–155.

60 51 G. W. Wagner, L. R. Procell, Y.-C. Yang and C. A. Bunton, *Langmuir*, 2001, **17**, 4809–4811.

65 52 I. A. Fallis, P. C. Griffiths, T. Cosgrove, C. A. Dreiss, N. Govan, R. K. Heenan, I. Holden, R. L. Jenkins, S. J. Mitchell, S. Notman, J. A. Platts, J. Riches and T. Tatchell, *J. Am. Chem. Soc.*, 2009, **131**, 9746–9755.

70 53 S. Franke, *Manual of Military Chemistry- Volume 1 Chemistry of Chemical Warfare Agent*, Report AD849866, Deutscher Hilitarverlag, [East] Berlin, 1967.

75 54 T. Sandmeyer, *Ber. Dtsch. Chem. Ges.*, 1886, **19**, 857–861.

80 55 T. Sandmeyer, *Ber. Dtsch. Chem. Ges.*, 1885, **18**, 1767–1769.

85 56 F. D. Chattaway and O. G. Backeberg, *J. Chem. Soc., Trans.*, 1923, **123**, 2999–3003.

90 57 R. Fort and L. Denivelle, *Bull. Soc. Chim. Fr.*, 1954, 1109–1115.

95 58 M. C. Taylor, R. B. MacMullin and C. A. Gammal, *J. Am. Chem. Soc.*, 1925, **47**, 395–403.

100 59 F. D. Greene, C.-C. Chu and J. Walia, *J. Org. Chem.*, 1964, **29**, 1285–1289.

105 60 P. S. G. Tassignon, D. de Wit, T. C. de Rijk and L. F. De Buyck, *Tetrahedron*, 1995, **51**, 11863–11872.

110 61 <https://www.thechemicalengineer.com/news/csb-releases-final-report-on-explosions-at-midland-resource-recovery-facility/>, (accessed October 26th 2021).

115 62 R. C. Godfrey, N. J. Green, G. S. Nichol and A. L. Lawrence, *Nat. Chem.*, 2020, **12**, 615–619.

120 63 K. De Bruycker, S. Billiet, H. A. Houck, S. Chattopadhyay, J. M. Winne and F. E. Du Prez, *Chem. Rev.*, 2016, **116**, 3919–3974.

125 64 Z. Wang, L. Zhu, F. Yin, Z. Su, Z. Li and C. Li, *J. Am. Chem. Soc.*, 2012, **134**, 4258–4263.

130 65 W. Yu, Y. Li and D. Li, *Synthesis*, 2017, **49**, 4283–4291.

135 66 F.-Q. Huang, J. Xie, J.-G. Sun, Y.-W. Wang, X. Dong, L.-W. Qi and B. Zhang, *Org. Lett.*, 2016, **18**, 684–687.

140 67 J. Ozawa and M. Kanai, *Org. Lett.*, 2017, **19**, 1430–1433.

145 68 M. H. Davey, V. Y. Lee, R. D. Miller and T. J. Marks, *J. Org. Chem.*, 1999, **64**, 4976–4979.

150 69 S. Iriuchijima and G. Tsuchihashi, *Tetrahedron Lett.*, 1969, **10**, 5259–5262.

155 70 V.-E. H. Kassin, R. Morodo, T. Toupy, I. Jacquemin, K. Van Hecke, R. Robiette and J.-C. M. Monbaliu, *Green Chem.*, 2021, **23**, 2336–2351.

160 71 B. Gutmann and C. O. Kappe, *J. Flow Chem.*, 2017, **7**, 65–71.

165 72 B. Gutmann, D. Cantillo and C. O. Kappe, *Angew. Chem., Int. Ed.*, 2015, **54**, 6688–6728.

170 73 D. Dallinger, B. Gutmann and C. O. Kappe, *Acc. Chem. Res.*, 2020, **53**, 1330–1341.

175 74 R. Morodo, R. Gérardy, G. Petit and J.-C. M. Monbaliu, *Green Chem.*, 2019, **21**, 4422–4433.

180 75 K. Wojciechowskl, *Org. Prep. Proced. Int.*, 1988, **20**, 493–496.

185 76 Y. Yuan, X. Shi and W. Liu, *Synlett*, 2011, 559–564.

190 77 G. W. T. M. J. Frisch, H. B. Schlegel, G. E. Scuseria, M. A. Robb, J. R. Cheeseman, G. Scalmani, V. Barone, B. Mennucci, G. A. Petersson, H. Nakatsuji, M. Caricato, X. Li, H. P. Hratchian, A. F. Izmaylov, J. Bloino, G. Zheng, J. L. Sonnenberg, M. Hada, M. Ehara, K. Toyota, R. Fukuda, J. Hasegawa, M. Ishida, T. Nakajima, Y. Honda, O. Kitao, H. Nakai, T. Vreven, J. A. Montgomery, J. E. Peralta Jr., F. Ogliaro, M. Bearpark, J. J. Heyd, E. Brothers, K. N. Kudin, V. N. Staroverov, T. Keith, R. Kobayashi, J. Normand, K. Raghavachari, A. Rendell, J. C. Burant, S. S. Iyengar, J. Tomasi, M. Cossi, N. Rega, J. M. Millam, M. Klene, J. E. Knox, J. B. Cross, V. Bakken, C. Adamo, J. Jaramillo, R. Gomperts, R. E. Stratmann, O. Yazayev, A. J. Austin, R. Cammi, C. Pomelli, J. W. Ochterski, R. L. Martin, K. Morokuma, V. G. Zakrzewski, G. A. Voth, P. Salvador, J. J. Dannenberg, S. Dapprich, A. D. Daniels, O. Farkas, J. B. Foresman, J. V. Ortiz, J. Cioslowski and D. J. Fox, *Gaussian09, Revision D.01*, Gaussian Inc., Wallingford (CT), 2009.

195 78 H. M. W. Mintz and C. , *Org. Synth.*, 1969, **49**, 9.

200 79 Y. H. Kim, S. C. Lim, H. R. Kim and D. C. Yoon, *Chem. Lett.*, 1990, **19**, 79–82.

1 80 K. R. Rao and P. B. Sattur, *J. Chem. Soc., Chem. Commun.*, 1989, **6**, 342–343.

5 81 J. Drabowicz, *Synthesis*, 1986, 831–833.

10 82 J. S. Grossert, W. R. Hardstaff and R. F. Langler, *J. Chem. Soc., Chem. Commun.*, 1973, **2**, 50a–50a.

15 83 M. Cinquini and S. Colonna, *Synthesis*, 1972, 259–260.

20 84 K. C. Tin and T. Durst, *Tetrahedron Lett.*, 1970, **11**, 4643–4644.

25 85 F. G. Mann and W. J. Pope, *J. Chem. Soc., Trans.*, 1922, **121**, 594–603.

30 86 J. S. Grossert, W. R. Hardstaff and R. F. Langler, *Can. J. Chem.*, 1977, **55**, 421–426.

35 87 F. Ruff, I. Jalsovszky, D. Szabó, J. Rábai, Ö. Farkas and Á. Kucsman, *J. Phys. Org. Chem.*, 2012, **25**, 1086–1096.

40 88 F. Ruff, D. Szabó, J. Rábai, I. Jalsovszky and Ö. Farkas, *J. Phys. Org. Chem.*, 2019, **32**, e4005.

45 89 N. Barnwell, P. Cornwall, D. Horner, J. Knott and J. Liddon, *Org. Process Res. Dev.*, 2010, **14**, 278–288.

50 90 C. Shen and K. L. Parkin, *J. Agric. Food Chem.*, 2000, **48**, 6254–6260.

55 91 E. L. Clennan, D. Wang, H. Zhang and C. H. Clifton, *Tetrahedron Lett.*, 1994, **35**, 4723–4726.

60 92 A. Banerjee, in *Encyclopedia of Reagents for Organic Synthesis*, DOI: [10.1002/047084289X.rn00895](https://doi.org/10.1002/047084289X.rn00895). Q14

Proof Central

Dear Author

Please use this PDF proof to check the layout of your article. If you would like any changes to be made to the layout, you can leave instructions in the online proofing interface. First, return to the online proofing interface by clicking "Edit" at the top of the page, then insert a Comment in the relevant location. Making your changes directly in the online proofing interface is the quickest, easiest way to correct and submit your proof.

Please note that changes made to the article in the online proofing interface will be added to the article before publication, but are not reflected in this PDF proof.